Metamorphic evolution of high-pressure Quartz Schists in the Zhan metamorphic complex, Sanandaj-Sirjan zone, Iran

Nayer Ajalli[1,]*, Javad Izadyar[1], Nazila Nasihatsheno[1]

1- Department of Geology, University of Zanjan, University Blvd., Zanjan, Iran.

* Corresponding Author: n.ajalli@yahoo.com

Received: 11 May 2014 / Accepted: 01 March 2015 / Published online: 12 March 2015

Abstract

The study area is located at the Sanandaj-Sirjan zone in the west and north-west of Azna and north-east of Doroud, Iran. The Quartz-Schists are divided into two main groups: amphibole-quartz schist and garnet-quartz schist. Field and microstructural studies show several deformational phases. The D1 episode which is represented by S1, matches with M1 metamprphism and D2 deformation matches with M2 metamorphism. Sodic-amphibole, phengite, garnet and plagioclase are the minerals of M1 metamorphism stage; and calsic-amphibole, garnet, plagioclase, muscovite, biotite and chlorite are the minerals of M2 metamorphism stage. The estimated P-T using Thermocalc indicates that minerals paragenesis in M1 stages have average temperature of 633±76 ◦C and also pressure of 15.2±1 Kbar; and in M2 stages have average temperature of 588±41 ◦C and also pressure of 6.8±1 Kbar. Based on calibration methods, minerals paragenesis in M1 stages have average temperature of 621±5 ◦C and also pressure of 14-16 Kbar and in M2 stages have average temperature of 546±91 ◦C and also pressure of 8.7-8.01 Kbar. Based on calibrated curves and thermocalc measurement the stability range of mineral paragenesis in M1 are in echlogitefacies and the stablility of mineral paragenesis in M2 are in amphibolite facies. This complex generated in subduction zone (Tethys under central Iran) in late Triassic and exhumed in Cretaceous and thrusted on Zagros during collision between Afro-Arabi and central Iran micro continent in Miocene.

Keywords: Petrology, Zhan complex, Sanandaj-Sirjan, Metamorphism, Quartz schist, Thermobarometry.

1–Introduction

Iranian crust constitutes one of the largest tectonic provinces in the southwestern Asia and is regarded as a complicated puzzle of continental fragments initially rifted from Gondwana which presently separated from each other by complex fold and thrust and discontinuous ophiolitic belts. These fragments arepresently separated by discontinuous ophioliticbelts (Stöcklin, 1968; Berberian and King, 198).Among these continental fragments, the Sanandaj-Sirjan zone (Stöcklin, 1968) is located between the Central Iran block or microplate, in the east, and the Zagros fold-thrust belt_ located on northeastern margin of the Arabian platform_on the west (Stöcklin, 1968; Alavi, 1994; Berberian, 1995; Ghasemi and Talbot, 2006) (Fig. 1). The Sanandaj-Sirjan zone stretches for 1500 km from northwest tosoutheast of Iran and is up to 200 km wide (Berberian, 1977; Mohajjel *et al*., 2003). It is divided into the “outer belt”, made by imbricatethrust slices (e.g. the Zagros suture), and the “innerbelt”, made mainly by

Mesozoicmetamorphicrocks (Mohajjel *et al*., 2003). The Sanandaj-Sirjan zone records amphibolite-facies metamorphic assemblage acquired during the Cretaceous-Tertiary continental collision between the Arabian andIranian continental plates (Şengör and Natal'in, 1996; Mohajjel *et al*., 2003).

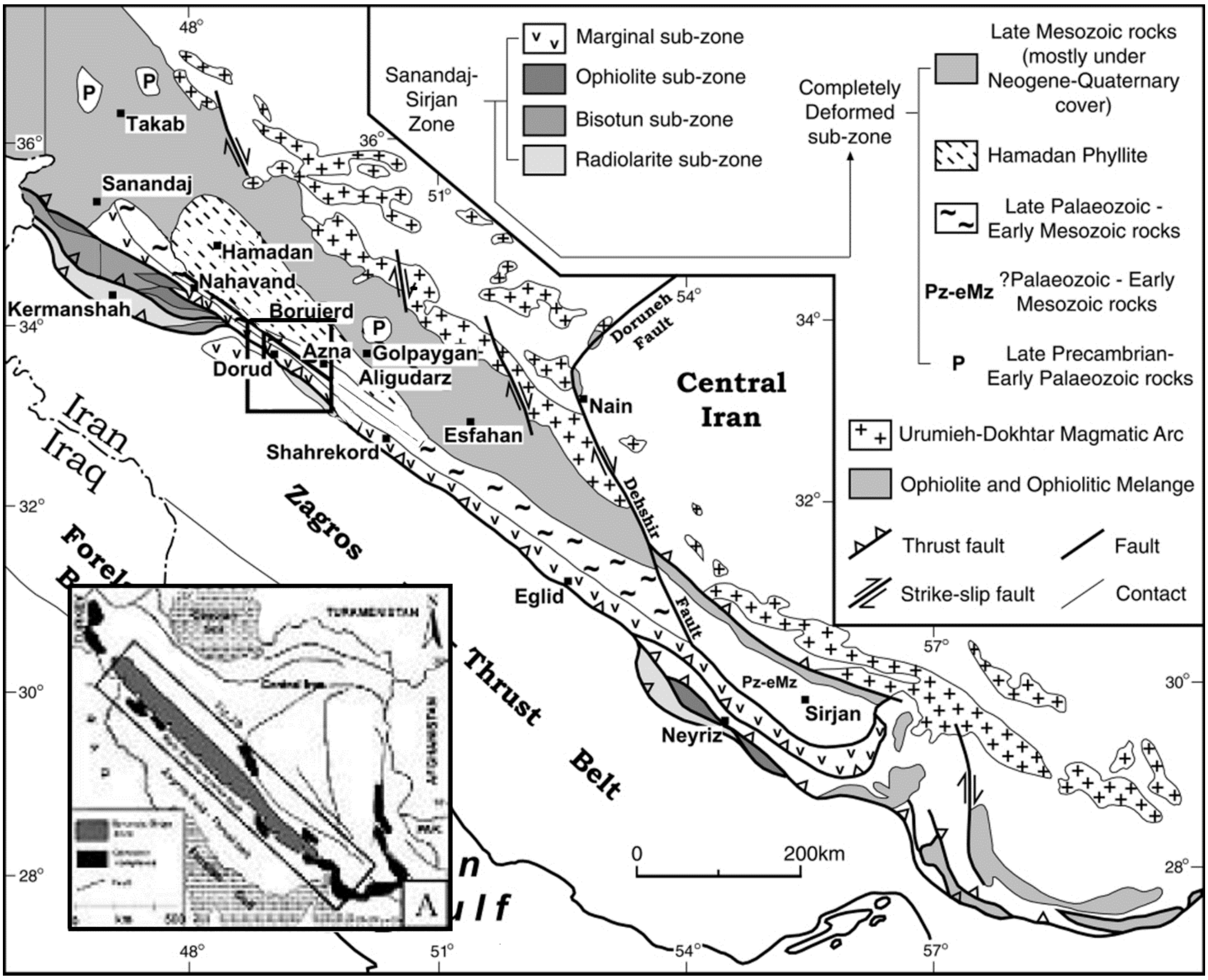

Figure 1) Simplified tectonic map of the Sanandaj-Sirjan zone (modified after Mohajjelet al., 2003).

From the southwest to the northeast, the Sanandaj-Sirjan zone consists of several elongated sub-zones: (1) the Radiolarite sub-zone made of Triassic-Cretaceous shallow marine limestone and dominantdeep-marine radiolarite; (2) the Bisotun sub-zonethat includes Late Triassic to Late Cretaceous limestone; (3) the Ophiolite sub-zone thatrepresents the Zagros suture zone; (4) the Marginalsub-zone that contains abundant Late Jurassic-Early Cretaceous. All sub-zones are imbricated in a complicate thrust system, with out-of-sequence thrusts that locally juxtaposes younger units over older ones. Major thrusting has affected Miocene marine rocks and involved Neogene conglomerate. Locally, allochthons of the Bisotun sub-zone and Marginal sub-zone have been thrust toward the southwest, above the Zagros fold-and-thrust belt during Late Tertiary compressive tectonics (Mohajjel *et al*., 2003).

The Zhan metamorphic complex is located in the Sanandaj-Sirjan structural zone (Complexly deformed sub-zone, SW Iran). In this paper, utilizing petrography, mineralogy and thermobarometer of quartz schists in the study area and using data from literature, we presented a hypothetic geodynamic evolution between Arabian and Iran continental margins and approximately the position of the subducted and exhumed Zhan metamorphic complex.

2–Geological Framework

Field investigations highlighted that the complex is made of four main groups of rocks: 1) philite and pelitic schist, 2) meta-dolomite and marble, 3) quartzite and quartz schist, 4) gneiss (Middle-Late Triassic).

We documented quartz schists in three parts of investigation field. The quartz schists of the center recorded S1 along N-S with 50-60º dip towards East, while the quartz schists of the north recorded S2 along NE-SW with 40-70º dip toward NE. The quartz-schists of the core of Bavaki anticline which show S1 along NE-SW are aligned with anticlines axial plane (Fig. 2).

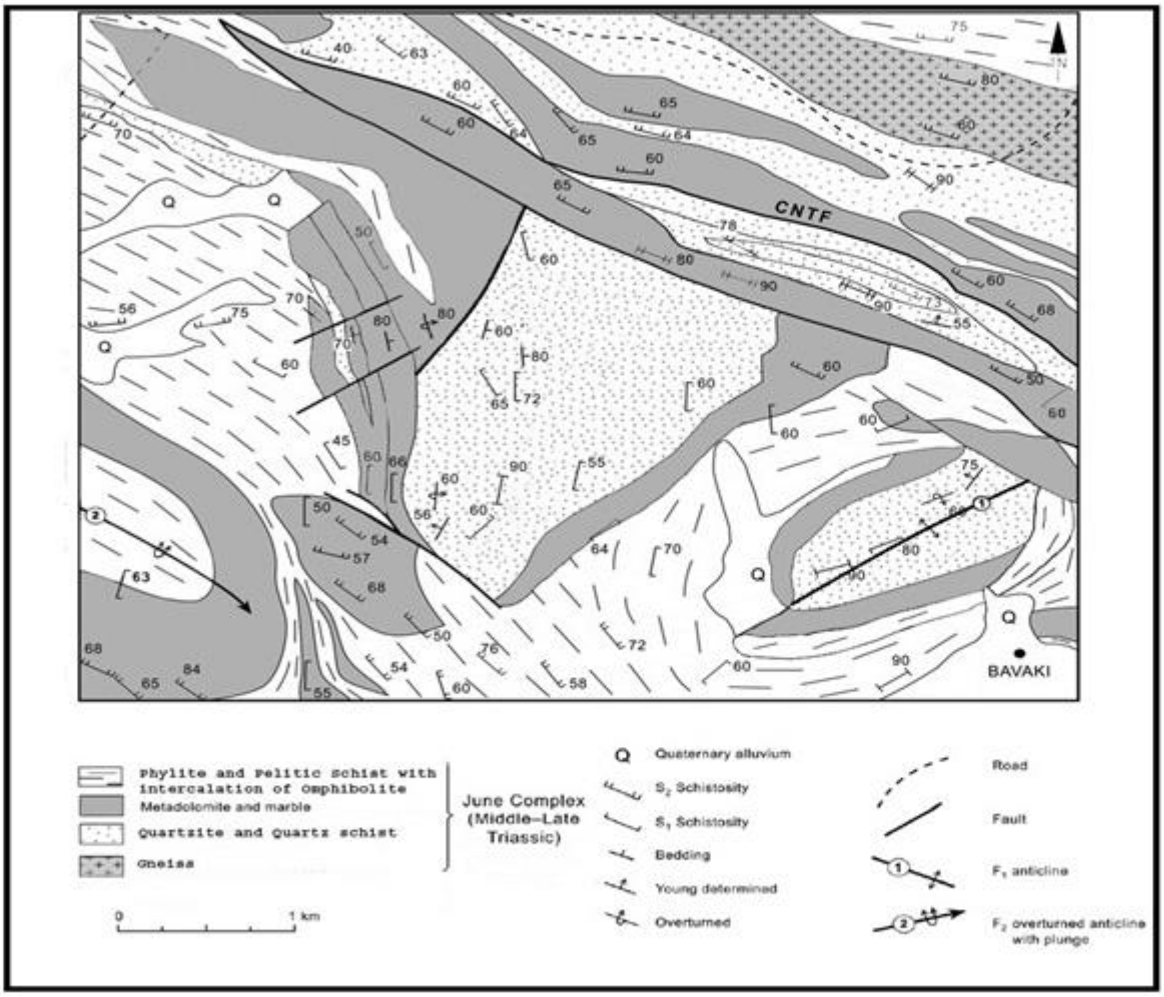

Figure 2) Geological sketch map of the Zhan metamorphic complex, Shazand city (modified after Sahandi and Radfar, 2006).

Philite and politic schists are found in the west of investigation field. Based on field data and chemical analyses, these rocks recorded S2 along NW-SE with 40-70º dip toward NE. The dominant schistosity of the marbles and meta-dolomites is S2 along NW-SE with 40-70º dip toward NE. Gneiss is recorded in the NE of investigating field. It shows S2 schistosity along NW-SE with 60-80º dip toward NE. These data was measured by compass in field investigation (Fig. 2).

3–Deformation and Petrography

D1 fabric, the eldest deformation of the Zhan complex, produced S1 Schistosity. D1 is locally transposed by the main regional deformation phase documented in the area (D2 phase). D2 phase produced F2 folds, visible both at outcrop and microscopic scale and a S2 foliation developed as an axial plane foliation. Mylonitic fabric has been also described in the quartz schists. It is marked by assymetrical pressure shadows, elongated albite and polycrystallines of quartz which are completely alongated through main schistosity.

D1 and D2 structures were deformed by a third deformation phase (D3) that produced S3. No metamorphic growth or recrystallizations have been documented during D3 deformation phase. The quartz schist consists of quartz, amphibole, garnet, white mica, biotite, plagioclase and chlorite.

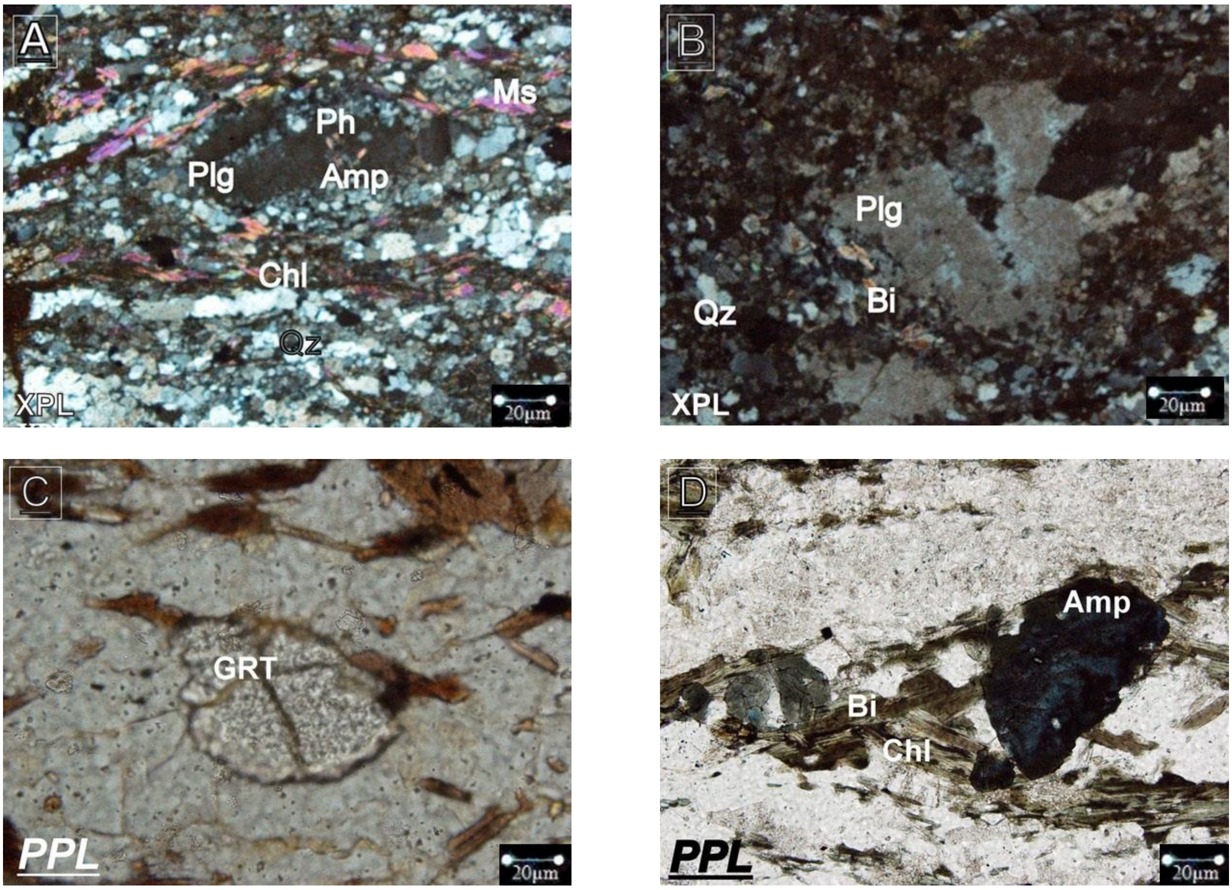

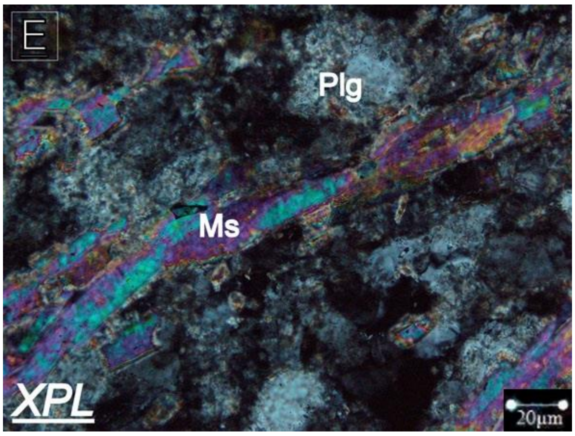

Figure 3) Photomicrographs of quartz schists from Zhan metamorphic complex. A) Inclusions in Plagioclase (Plg). B) Zoning structure in Plagioclase (Plg). C) Blasts of garnet (Grt) without Inclusion. D) Zoning structure in Amphibole (Amp). E) Chemical zoning in White mica which its core is phengite (Ph) and is rimmed by muscovite (Ms). (Mineral name abbreviations from Kretz, 1983).

Phengite and sodic amphibole without chemical zoning structure are preserved in the core of plagioclase. They have developed during D1 deformation phase. Plagioclase shows chemical zoning which shows from core to the rim an increase in albite and a decrease in anortite (Fig. 3A, B).The blasts of garnet in quartz schists have no inclusion trails and have no relative structure with the main regional schistosity (Fig. 3C).

Two different occurrences of amphibole can be identified: 1) amphibole in the matrix occurring in S2 schistosity, 2) amphibole, included in plagioclase core without chemical zoning structure. Amphibole that occurs in matrix with chemical zoning usually have sodic composition rimmed by calcic amphibole. Amphiboles preserved within the core of albite porphyroblast show a homogenous sodic composition (Fig. 3D). Two types of white micas can be distinguished: 1) white mica in the matrix or following the S2 schistosity; 2) white mica included in plagioclase core. White mica that occurs in matrix shows chemical zoning in which its core is phengite and is rimmed by muscovite. In addition some of the white micas in the matrix are altered to chlorite. White mica that occurs in the core of albite porphyroblast has phengite composition (Fig. 3E). Chlorite and biotite have no chemical zoning structure. They follow the S2 schistosity and by muscovites made the main schistosity of quartz schists. Table 1 shows these relations.

Table 2) Representative microprobe analyses of garnet.

location Point No.	Core 46-3-1	Rim 46-3-2	Core 46-3-3	Rim 46-3-4	Core 46-3-5	Rim 46-3-6	Core 46-3-7	Rim 46-3-8
SiO2	36.88	36.65	37.66	37.06	39.01	38.35	39.21	38.47
TiO2	0.06	0.07	0.02	0.01	0.10	0.09	0.08	0.09
Al2O3	20.67	20.48	20.98	20.16	21.61	21.451	21.53	21.62
FeO	32.10	32.76	27.29	31.30	23.12	25.30	23.41	25.23
MnO	0.30	0.62	0.91	3.22	1.21	7.43	2.17	6.17
MgO	3.93	2.65	4.56	5.03	5.86	2.64	5.75	3.53
CaO	3.57	6.85	8.19	3.31	9.75	4.81	8.12	5.21
Na2O	0.03	0.03	0.07	0.04	0.02	0.03	0.04	0.02
K2O	0.01	0.01	0.01	0.00	0.00	0.00	0.01	0.00
Total	99.98	99.97	99.93	99.93	99.96	99.91	99.93	99.94
Si	2.950	2.911	2.962	2.940	2.997	3.041	3.029	3.027
Ti	0.004	0.004	0.001	0.001	0.006	0.005	0.005	0.005
Al	1.950	1.965	1.945	1.885	1.957	2.005	1.961	2.006
Fe2+	1.966	2.149	1.654	1.836	1.444	1.678	1.512	1.660
Mn	0.020	0.042	0.061	0.216	0.079	0.499	0.142	0.411
Mg	0.469	0.314	0.534	0.595	0.671	0.312	0.662	0.414
Ca	0.583	0.306	0.690	0.281	0.803	0.409	0.672	0.439
Na	0.005	0.005	0.011	0.006	0.003	0.005	0.005	0.006
K	0.001	0.001	0.001	0.000	0.000	0.000	0.001	0.000
Total	8.00	8.00	8.00	8.00	8.00	7.95	7.99	7.96

4–Mineral Chemistry

Mineral analysis was performed with a camera SX100 electron probe microanalyzer (10KV, 10 nA) as standards in KMA (Knowledge Monitoring Assessment) research group in Malaysia.

4.1- Garnet

Within the different microstructural domains, garnets show similar chemical compositions. They show: (1) almandine-rich composition, and (2) concentrically zoning with core relatively richer in pyrope and grassolar and poorer in almandine and spessartine. For example, the garnet shows, from the core to the rim, an increase in spessartine and almandine components and a decrease in pyrope and grossular contents (Table 2, Fig. 4).

4.2- Amphibole

According to the IMA classification scheme (Leak *et al*., 1997), we documented two main amphibole groups: (1) sodic amphiboles such as nebolite and Fe-nebolite, and (2) calcic amphiboles such as edenite and magnesio hornblende (Table3, Fig. 5). Amphiboles in the matrix contain two chemical zoning. Their cores show nebolite and Fe-nebolite composition, whereas their rims have edenite and magnesio-hornblende composition. We documented that calcis amphibole grew exclusively as rim around sodic amphibole. This data shows that the core grew close to, or during the metamorphic peak conditions, whereas the rims developed during retrograde metamorphic condition was formed probably during the D2 deformation. Amphiboles that occure in the core of albite porphyroblast also show sodic composition.

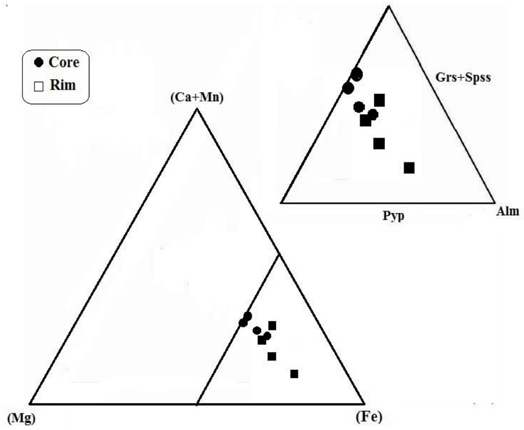

Figure 4) Garnet compositions plotted on (Mn+Ca)-Fe^{2+}-Mg diagrams.

4.3- White mica

White micas analysis are listed in table (4). White mica along with S2 schistosity shows variation compositional from core to the rim. Micas core composition deviates by tschermsk substitution ($MgSi=Al_{-1}Al_{-1}$) from ideal muscovite end-member composition toward celadonite (Table 4, Fig. 6). Micas rim composition is close to ideal muscovite end-member. White micas preserved as inclusion in the core of plagioclase show a homogeneous composition deviates by tschermak substitution ($MgSi=Al_{-1}Al_{-1}$) from ideal muscovite end-member. An enrichment of celadonite component indicates an increase of pressure (Vidal and Parra, 2000). Therefore, an increase in ideal muscovite end member and decrease in celadonite component that documented from the core to the rim in white micas along with S2 schistosity shows that they grew during a decompressive metamorphic condition in which the D2 deformation phase occurred during the lowest pressure condition (Fig. 6).

4.4- Chlorite

Representative analysis of chlorite are listed in Table 5. Chlorite composition deviates from ideal clinochlore end-member towards amesite by tschermak substitution (MgSi=Al-1Al-1), towards daphnite by Fe^{+2}=Mg^{+2} substitution, and towards sudoite by di/trioctahedral substitutions (Fig. 7).

4.5- Biotite

Microprobe analysis of biotite are provided in Table 6. On the average, the phlogopite and annite end members made up the most percentage of biotite composition.

4.6- Plagioclase

Microprobe analysis of plagioclase shows that plagioclase with chemical zoning from the core($An_{60\%}$, $Ab_{40\%}$) to the rim($An_{35\%}$, $Ab_{65\%}$) becomes richer in albiteand poorer in anortite end members.

5–Metamorphism and P-T conditions

Mineral chemistry and microstructural investigations results indicate that quartz schists in the Zhan complex record two events of metamorphism. The first metamorphic stage (M1) is characterized by mineral assemblage of garnet, phengite, sodic amphibole, plagioclase that indicated eclogitefacies.

The second metamorphic stage (M2) can be recognized by mineral assemblage like calcic amphibole, garnet, plagioclase, muscovite, biotite and chlorite that produced during D2 episode of deformational phase and demonstrated in amphibolites facies.

In order to constrain the P and T conditions recorded by the quartz schists during M1 and M2 metamorphic events, we defined the microstructural domains where mineral assemblages are close to metamorphic equilibrium. Then to obtain a solid and robust dataset, we applied different thermodynamic methods. To estimate P and T representative for each metamorphic phase, we used the mean mineral compositions.

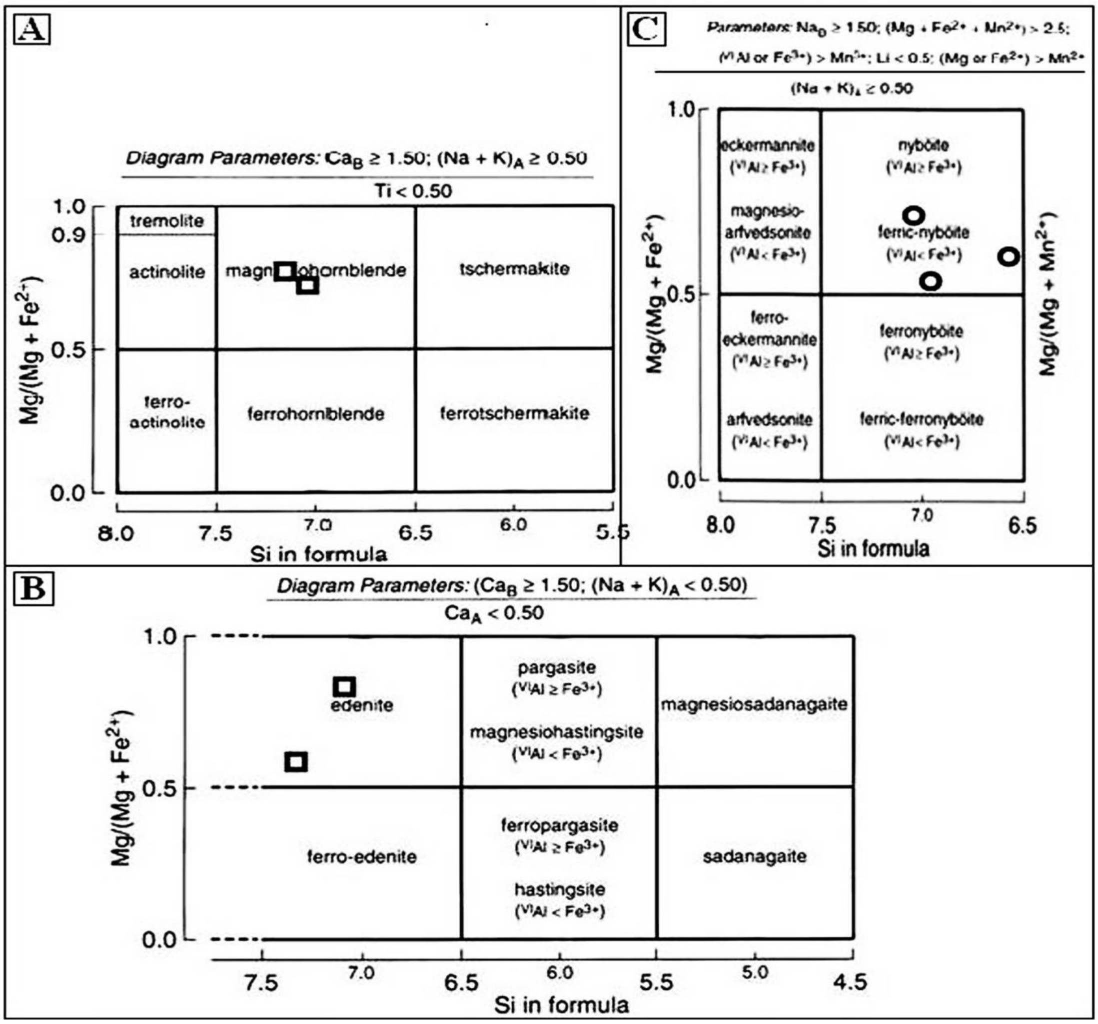

Figure 5) Composition diagrams for calcic (A, B) and sodic (C) amphiboles (Leak et al., 1997).

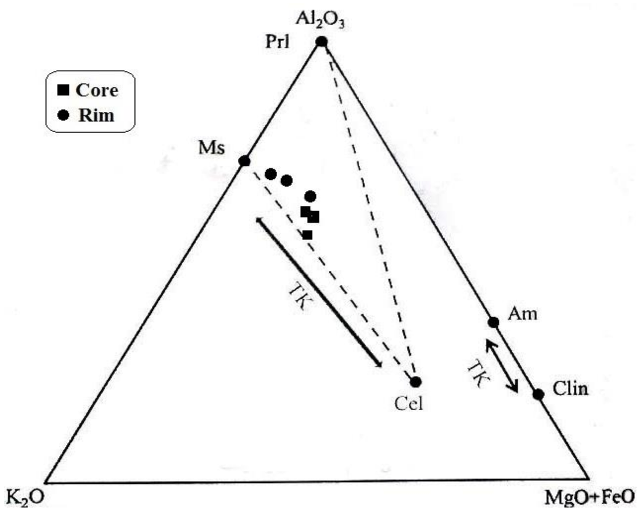

Figure 6) Mineral composition of white mica in diagram of (K_2O, Al_2O_3, MgO+FeO) amesite (Am), clinochlore (clin), celadonite (cel), pyrophilte (prl), tschermakit (TK) (Vidal and Parra, 2000).

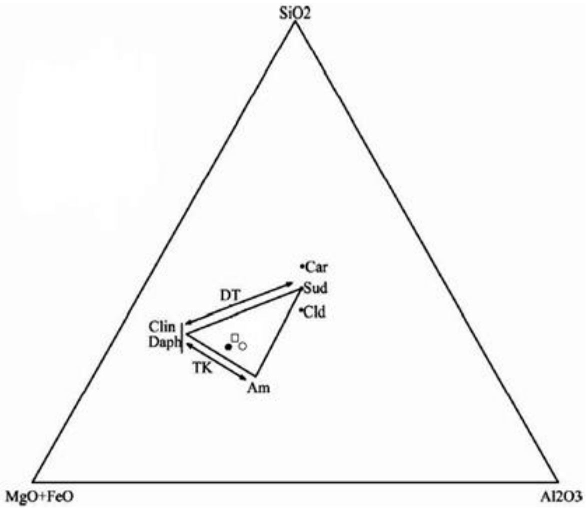

Figure 7) Mineral compositions of chlorite, amesite (Am), clinochlore (clin), aphenite (Daph), Sudoite (Sud), tschermakit (TK), di/trioctahedral (DT), (SiO_2, Al_2O_3, MgO+FeO) (Vidal and Parra, 2000).

Table3) Representative microprobe analyses of amphibole.

Point No.	Core 42-4-9	Rim 42-4-10	Core 42-4-11	Rim 42-4-12	Core 42-10-13	Rim 42-10-14	Core 42-10-15	Rim 42-10-16	Inclusion of amphibole 42-4-17	Inclusion of amphibole 42-4-18
SiO2	43.53	50.43	48.82	50.23	48.14	50.13	47.55	50.61	49.13	48.56
TiO2	0.68	0.41	0.31	0.1	0.50	0.43	0.13	0.37	0.13	0.23
Al2O3	16.07	6.02	16.21	6.13	15.85	6.17	15.12	5.13	14.18	15.71
FeO	12.63	8.96	10.62	7.807	11.25	8.15	12.02	9.13	11.30	11.08
MnO	0.00	0.05	0.10	0.09	0.10	0.08	0.09	0.10	0.3	0.08
MgO	8.72	16.82	8.33	17.14	7.82	17.23	9.12	16.25	10.71	9.84
CaO	8.05	12.56	7.21	12.15	7.35	12.87	7.54	12.21	7.33	7.79
Na2O	5.80	1.41	4.21	1.65	6.12	2.02	5.62	3.12	4.95	5.01
K2O	0.62	0.51	0.7	0.4	0.51	0.33	0.43	0.21	0.36	0.37
Total	96.10	97.90	96.51	96.77	97.64	97.41	97.62	97.13	98.39	98.67
Si	6.472	7.218	7.000	7.235	6.905	7.191	6.85	7.320	6.972	6.865
Ti	0.076	0.044	0.033	0.011	0.054	0.046	0.014	0.040	0.014	0.024
Al	2.817	1.016	2.740	1.041	2.680	1.043	2.57	0.875	2.372	2.618
Fe2+	1.57	1.072	1.274	0.940	1.350	0.978	1.44	1.104	1.341	1.310
Mn	0.00	0.006	0.012	0.011	0.012	0.010	0.011	0.012	0.036	0.010
Mg	1.93	3.58	1.780	3.679	1.672	3.683	1.95	3.503	2.265	2.073
Ca	1.28	1.92	1.108	1.875	1.13	1.97	1.16	1.892	1.115	1.180
Na	1.67	0.39	1.17	0.46	1.70	0.56	1.57	0.87	1.36	1.373
K	0.11	0.09	0.128	0.074	0.093	0.060	0.079	0.039	0.065	0.067
Total	15.93	15.46	15.24	15.48	15.59	15.55	15.67	15.66	15.54	15.52

Table4) Representative microprobe analyses of muscovite.

Point No	Core 42-8-19	Rim 42-8-20	Core 42-8-21	Rim 42-8-22	Core 42-9-23	Rim 42-9-24	Ms $42\text{-}9\text{-}24_1$	Ms 42-9-25	Inclusion of muscovite 42-4-26	Inclusion of muscovite 42-4-27
SiO2	49.72	45.92	48.31	48.05	49.05	48.03	47.31	47.25	48.16	49.02
TiO2	0.25	0.10	0.27	0.51	0.37	0.43	0.41	0.31	0.38	0.09
Al2O3	28.17	34.47	27.41	34.01	27.66	34.23	34.72	34.63	31.70	28.31
FeO	3.61	2.99	4.35	2.12	3.17	1.53	2.12	3.01	1.16	4.34
MnO	-	-	-	-	-	-	0.02	0.01	0.01	0.01
MgO	3.35	3.24	4.12	1.65	4.02	1.17	1.14	1.13	2.67	3.05
Na2O	0.45	1.16	0.47	0.32	0.57	0.41	0.37	0.27	0.95	0.60
K2O	9.94	9.58	9.93	9.76	9.95	9.83	9.85	9.75	9.32	10.0
Total	95.77	97.69	95.20	96.59	94.98	95.63	96.09	96.59	94.42	95.76
Si	3.305	3.000	3.253	3.139	3.290	3.165	3.110	3.098	3.210	3.275
Ti	0.012	0.005	0.014	0.025	0.019	0.021	0.020	0.015	0.019	0.005
Al	2.208	2.655	2.176	2.619	2.187	2.659	2.691	2.677	2.49	2.230
Fe2+	0.060	0.049	0.074	0.035	0.053	0.084	0.040	0.050	0.028	0.073
Mn	-	-	-	-	-	-	0.001	0.001	0.001	0.001
Mg	0.332	0.315	0.414	0.161	0.402	0.115	0.112	0.110	0.265	0.304
Na	0.058	0.147	0.061	0.041	0.066	0.052	0.047	0.34	0.123	0.078
K	0.843	0.798	0.853	0.813	0.852	0.826	0.826	0.816	0.792	0.852
Total	6.95	7.08	7.017	6.91	6.99	6.92	6.92	6.91	6.96	6.98

For the garnet, white mica, amphibole and plagioclase with compositional zoning, the core compositions were used to estimate the P-T conditions of M1 metamorphic event while their rim compositions were utilized for P-T estimates of M2 metamorphic event (Table 8). Thermobarometry on M1 and M2 metamorphic events was mostly performed using calibrated geothermobarometers and the THERMOCALC 3.26 program (Powell *et al*., 1988) in average PT mode with the self-consistent thermodynamic dataset of Holland and Powell (1998). Temperature of M1 metamorphic event was estimated using different calibrations of geothermometers based on the Fe-Mg partitioning between garnet and phengite (Krogh *et al*., 1978; Green *et al*., 1982). Temperature estimates 619-624 °C obtained from Fe-Mg thermometer between garnet core and phengite. Pressure of M1 metamorphic event was estimated using the phengite barometer of Massone and Schreyer (1987). Assuming Si=3.5 and temperature of 620°C, in fact, we obtained a maximum pressure of 1.5 Gpa. The average P-T estimates obtained using THERMOCALC yield T = 633±76 ºC and P = 1.52±1 GPa (Table 8).

Temperature of M2 metamorphic event was estimate using garnet-hornblende geothermometer (Graham and Powell, 1984) and different calibrations of geothermometers based on the Fe-Mg partitioning between garnet-biotite (Thompson, 1976; Hold *et al*., 1977; Ferry *et al*., 1978). Temperature estimates range from 546.91°C from garnet-hornblende thermometer to 546-604°C from Fe-Mg thermometer between garnet and biotite. Pressure of M2 metamorphic event was estimated using the Grt-Hbl-Plg-Qtz barometer of Kohn and Spear (1989) and using Grt-plg-Ms-Bi barometer of Hodges and crowley (1985). Pressure estimates range from 0.80 to 0.87 Gpa (Table 9).

Table 5) Representative microprobe analyses of chlorite.

Point No.	**41-1-28**	**41-1-29**	**41-1-30**
SiO2	23.09	24.90	25.23
TiO2	0.04	0.03	0.12
Al2O3	21.42	20.60	20.73
FeO	29.90	26.88	22.83
MnO	0.12	0.06	0.14
MgO	10.80	13.50	16.76
Total	86.56	85.97	86.50
Si	2.552	2.704	2.671
Ti	0.003	0.002	0.010
Al	2.791	2.637	2.587
Fe2+	2.76	2.441	2.024
Mn	0.011	0.006	0.013
Mg	1.779	2.185	2.644
Total	10	9.97	10

Average P-T estimates obtained from THERMOCALC are T=588±41°C and P=6.8±1 GPa. We estimated that the quartz schists from the Zhan complex reached depth of at least 64 Km, corresponding to a geothermal gradient of almost 7-8° C/Km. According to thermobaric calculations, we documented a retrograde path from an eclogite to amphibolite- facies conditions (Fig. 8). As the M2 metamorphic assemblage occurred during the retrograde path, the D2 penetrative fabrics were acquired during the exhumation of the Zhan complex.

Table 6) Representative microprobe analyses of biotite.

Point No	**42-3-37**	**42-3-38**	**42-3-39**	**42-3-40**
SiO2	35.98	36.76	36.65	36.53
TiO2	1.96	1.51	1.75	1.83
Al2O3	16.29	16.27	16.12	15.97
FeO	19.82	19.44	19.14	17.98
MnO	0.13	0.09	0.14	0.18
MgO	11.77	11.06	11.23	11.86
K2O	9.56	9.25	9.37	9.65
Total	95.73	94.39	94.40	94.00
Si	2.732	2.822	2.814	2.809
Ti	0.112	0.087	0.101	0.106
Al	1.458	1.472	1.459	1.448
Fe2+	1.129	1.244	1.229	1.156
Mn	0.008	0.006	0.000	0.012
Mg	1.332	1.265	1.285	1.359
K	0.926	0.006	0.918	0.947
Total	7.82	7.80	7.81	7.83

Table 7) Representative microprobe analyses of plagioclase.

Mineral	**Core**	**Rim**	**Core**	**Rim**	**Core**	**Rim**
Point No.	**41-1-28**	**41-1-29**	**41-1-30**	**41-1-31**	**41-1-32**	**41-1-33**
SiO2	54.34	58.47	55.21	57.31	55.31	58.26
Al2O3	29.77	27.06	29.62	26.75	29.51	27.13
CaO	11.18	8.07	10.98	8.13	11.02	8.15
Na2O	4.58	7.05	5.02	7.16	4.73	6.83

K2O	0.09	0.14	0.10	0.15	0.08	0.13
Total	99.90	99.97	99.93	99.50	99.96	99.50
Si	2.446	2.593	2.461	2.580	2.469	2.590
Al	1.577	1.415	1.556	1.420	1.553	1.442
Ca	0.539	0.384	0.526	0.392	0.527	0.388
Na	0. 400	0.606	0.434	0.625	0.409	0.589
K	0.005	0.008	0.006	0.009	0.005	0.007
Total	4.96	5.00	4.98	5.02	4.99	4.96

6–Metamorphism and P-T conditions

Our new structural and metamorphic data discussed above, coupled with other works carried out indifferent parts of the Sanandaj-Sirjan zone (Mohajjel *et al*., 2003; Agard *et al*., 2005; Agard *et al*., 2006; Ghasemi *et al*., 2006; Sheikholeslami *et al*., 2008) allow us to suggest a geodynamic scenario which can explain the complex geological evolution recorded in the area during the rifting andthe subsequent subduction and continental collision between Arabian and Iranian continental plates during Paleozoic up to Cenozoic (Fig. 9).

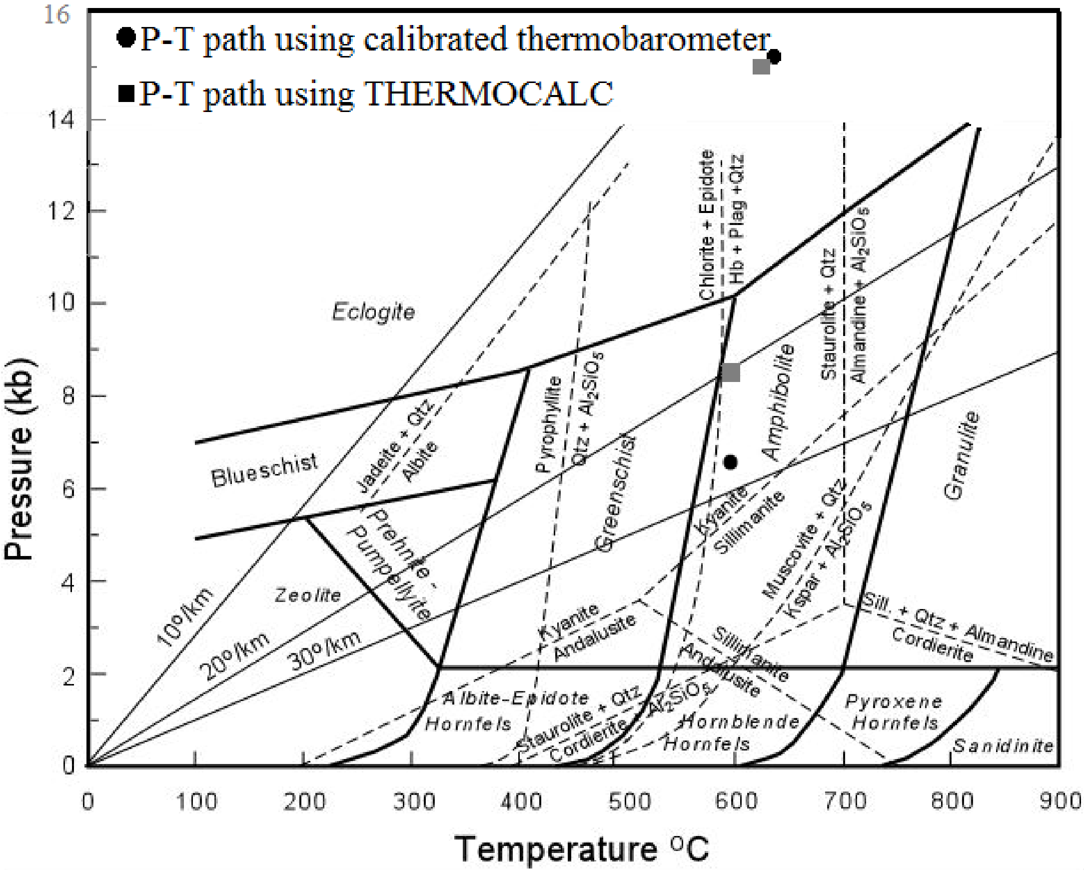

Figure 8) Petrogenetic gird and P-T paths for the Zhan metamorphic complex by thermobarometer and THERMOCALC calculations (Nelson et al., 2004).

According to Berberian and King (1981), during the subduction of the Hercynian or Paleotethys oceanic crust at the northern part of Iran microplate, a new rift, localized approximately at the present locationof the main Zagros thrust was generated. This rifting led to the formation of the Neotethys ocean and the movement towards north of the Iranian microplate. From Permian to Triassic, two main stages of rifting have been suggested (Mohajjel *et al*., 2003; Ghasemi *et al*., 2006). The first stage started probably during Permian in the Zagros basin andwas followed during Late Permian by wide basalt activity along the Sanandaj-Sirjan zone (Ghasemi *et al*., 2006). The second rifting stage started during Triassic and has been well described in thenorth-western sector of the Sanandaj-Sirjan zone where Triassic continental and shallow marine sedimentary successions were interrupted by wide spread basaltic magmatic activity with tholeitic affinity (Alavi *et al*., 1994).

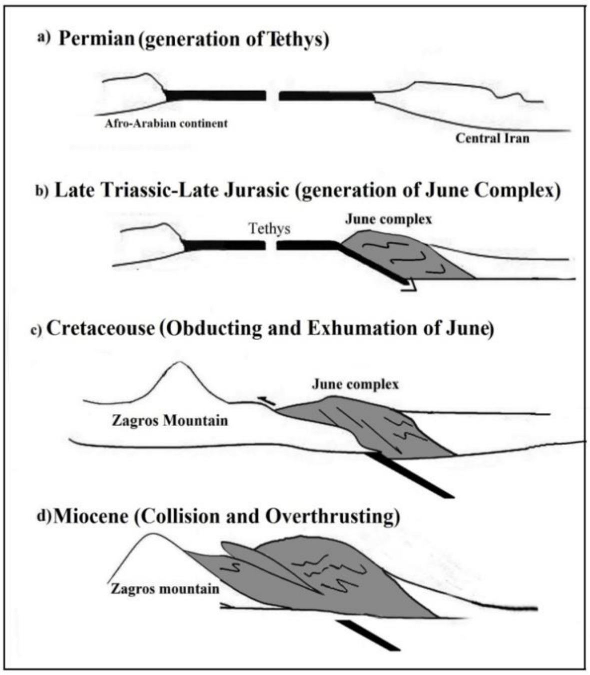

Figure 9) Hypothetic geodynamic evolution between Arabian and Iran continental margins deduced from our data and from literatures (modified after Agard et al., 2005). Filled and open stars represent approximately the position of the subducted and exhumed Zhan metamorphic complex, respectively.

The Jurassic metamorphism coupled with the magmatic activity documented along the southern sector of the Sanandaj-Sirjan zone, indicate that the subduction of Neotethyan oceanic crust beneath thesouth of Sanandaj-Sirjan zone may have already started during Late Jurassic-Cretaceous (Ghasemi *et al*., 2006). However, geochemical studies onvolcanic rocks in the ophiolitic complexes in the Zagros orogenic belt (Ghazi *et al*., 1999), indicate that most of them were generated in anintra-oceanic island arc environment, developed asconsequence of the ocean-ocean subduction during Early-Middle Jurassic. Intra-oceanic island arc in the Neotethys ocean was then obducted onto the north eastern margin of the Arabian plate (Ghasemi *et al*., 2006) (Fig. 9). According to Şengör and Natal'in (1996), subduction is a long-lived process that started fromthe Middle Jurassic and continued to the Early Miocene. Mohajjel *et al*. (2003) instead, suggested that the convergent regime developed for a longerperiod of time, spanning from Jurassic up to Cretaceous whereas Berberian and King (1981) studying igneous sequences adjacent to the north eastern Sanandaj-Sirjan zone suggested that the subduction process occurred during the Jurassic-Quaternary interval (Fig. 9). In this view, the high-pressure metamorphic conditions documented in the Zhan metamorphic complex (M1 metamorphism–D1 deformation) can be interpreted as the result of the Neotethyan oceanic lithosphere subduction under the Iranian continental plate during the Early-Middle Jurassic.

The main event of ophiolitic obduction on the north eastern margin of the Arabian peninsula occurred during 100-70 Ma (Mohajjel *et al*., 2003; Agard *et al*., 2005) (Fig. 9). On the basis of radiometric age carried out in the Zagros blueschists (Agard *et al*., 2005), they inferred that the ophiolitic sequences in the Sanandaj-Sirjan zone were exhumed by a modification of the mechanical coupling between the upper and lower plate inresponse to obduction process. This exhumation process was short-lived and stopped at around 80 Ma, before the continental collision between the Arabia and Iran continental (Agard *et al*., 2006).

Table 8) Estimated geothermobarometry for M1 metamorphic stages using different thermometers and barometers.

M1		Method
T (°C)	P (Kb)	
-	14	Phengite Barometry Massone and Schryer (1987)
-	16	Phengite Barometry Coggon and Holland(2002)
619.41	-	Garnet-Phengite Green-Hellman (1982)
624	-	Garnet- Phengite Krogh and Raheim (1978)

Coupling tectono-metamorphic investigations and geochronological analyses, Sheikholeslamei *et al.* (2008) suggested that exhumation of the metamorphic rocks in the Neyriz metamorphic complex (located at the southeastern sector of the Sanandaj-Sirjan zone) have been occurred during Jurassic. In the studied area, the exhumation process was short lived and finished before the end of Jurassic (Ghasemi *et al*., 2005) (Fig. 9). The exhumation of the Zhan metamorphic complex occurred through a decompressive and nearly isothermal path to the upper structural levels, where quartz schists recorded P = 0.80 – 0.87 GPa and T = 546 – 604 °C (M2 metamorphism - D2 deformation). This exhumation was due to the activation of the D2 shear belt probably in a transpressive regime. Paleogeographic reconstruction of Neotethys, infact, shows that Neotethys remained open along the Zagros suture untill Eocene or Miocene (Şengör *et al*., 1996). The timing of Neotethys closure along the Zagros suture, however remains a point ofdebate. Some authors suggest that the continental collision occurred during the Late Cretaceous (Berberian *et al*., 1981; Alavi, 1994) where asalternative model suggests that the continental collision along the Zagros suture occurred during Miocene (Şengör *et al*., 1996; Agard *et al*., 2005).

Table 9) Estimated geothermobarometry for M2 metamorphic stages using different thermometers and barometers.

M2		Method
T (°C)	**P (Kb)**	
594	-	Garnet-Biotite Thompson (1976)
593.95	-	Garnet-Biotite Hold/lee (1977)
604	-	Garnet-Biotite Ferry/ Spear (1978)
596	-	Garnet-Biotite Perchuk, L.L (1983)
582	-	Garnet-Biotite Dasgupta et al. (1991)
546.91		Garnet-Hornblend Graham and Powell (1984)
	8.7	Grt-Hbl-Plg-Qtz Kohn and Spear (1989)
-	8.01	Grt-Plg-Mus-Bio Hodges and Crowley (1985)

In the Zhan area, the Paleocene-Eocene sedimentary successions were deformed by foldsthat show similar orientation and geometry to F3 folds documented in the Zhan metamorphic complex. As a consequence, we suggest that these sedimentary successions have been deposited on thestill active Iranian margin and that oceanic closureand continental collision must have taken during Oligocene-Miocene.

7–Conclusions

The most important results of our investigation are: 1- Quartz schists of the Zhan metamorphic complex, record a polyphase tectono-metamorphic evolution. Relicts of D1 deformation phase are preserved as inclusion trails in the core of plagioclase crystals and in the core of zoning structures of Garnet, Plagioclase, amphibole and white mica. Whereas D2 deformation, the pervasive deformation of the area, produced a penetrative S2 axial plane foliation, a weakly and poor developed mylonitic foliation and F2 folds. D1 and D2 structures are themselves deformed by a post-Eocene deformation phase (D3) that produced S3 crenulation cleavage and F3 folds with NW-SE trending axis. 2- Two main metamorphism can be documented: (1) relicts of high-pressure metamorphic mineral assemblage (M1) such as phengite + garnet + sodic + amphibole + plagioclase, has been documented along S1 foliation and preserved as inclusions in the core of plagioclase, whereas a later amphibolite-facies metamorphism (M2) occurred during the D2 deformation phase. No metamorphic growth event has been documented during D3 deformation phase. 3- During the Early-Middle Jurassic, the Zhan complex belonging to the southern margin of the Iranian plate was involved in an accretionary prism and recorded a maximum pressure of 1.52 GPa and temperature of 624 - 619 °C (M1 metamorphism - D1 deformation). After this high-pressure event, the activation of the D2 shear belt (probably during a transpressive regime) was responsible for exhumation of quartz schists. The exhumation occurred through a decompressive and nearly isothermal path to the upper structural levels, where quartz schists recorded P = 0.87 – 0.80 GPa and T = 546 – 604 °C (M2 metamorphism – D2 deformation event) probably before the end of Cretaceous..

Acknowledgments:

We are most thankful to the University of Zanjan for the financial support of this study. The authors appreciate Dr. M. Balaghi, Dr. J. Deng and an anonymous reviewerfor their comments which help them to improve manuscript.

References:

Agard, P., Omrani, J., Jolivet, L., Mouthereau, F. 2005. Convergence history across Zagros (Iran): constraints fromcollisional and earlier deformation. International Journal of Earth Sciences**:** 94, 401–419.

Alavi, M. 1994. Tectonics of the Zagros orogenic belt of Iran: new data and interpretations. Tectonophysics: 229, 211–238.

Alavi, M., Mahdavi, M. A. 1994. Stratigraphy and structure of the Nahavand region in western Iran and theirimplications for the Zagros tectonics. Geological Magazine: 131, 43–47.

Berberian, M. 1977. Three phases of metamorphism in Haji-Abad quadrangle (southern extremity of Sanandaj-Sirjan structural zone): a palaeotectonic discussion. In: Berberian, M. (Ed.), Contribution to the seismotectonics of Iran (part3). Geological Survey of Iran, Tehran, Iran, 239–263.

Berberian, M., King, G.C. 1981. Towards a paleogeography and tectonics evolution of Iran. Canadian Journal of Earth Sciences: 18, 210–265.

Berberian, M. 1995. Master blind thrust faults hidden under the Zagros folds: active basement tectonics and surface morphotectonics. Tectonophysics: 241, 193–224.

Coggon, R., Holand T. J. B. 2002. Mixing properties of phengite micas and revised garnet-phengitethermobarometry. Journal of Metamorphic Geology: 20, 683–696.

Dasgupta, S., Sengupta, P., Fukulka, M., Bhattacharya, P. K. 1991. Journal of Geology: 99, 124–33.

Ferry, J. M., Spear, F. S. 1978. Contrib. Mineral. Petrol. 66, 113–7.

Ghazi, A. M., Hassanipak, A. A. 1999. Geochemistry of subalkaline and alkaline extrusives from the Kermanshah ophiolite, Zagros Suture Zone, Western Iran: implications for Tethyan plate tectonics. Journal of Asian Earth Sciences: 17, 319–332.

Graham, C. M., Powell R. 1984. A garnet-hornblende geothermometer: calibration, testing, and application to the pelona schist. Journal of Metamorph Geology:2, 13–31.

Green, T. H., Hellman, P. L. 1982. Fe- Mg partitioning between coexisting garnet and phengite at high pressure, and comments on a garnet- phengitegeothermometer. Lithos: 15, 253-266.

Hodges, K. V., Crowley, P. D. 1985. Error estimation and empirical geothermoborometry for pelitic systems. American Mineralogist: 70, 702–709.

Kretz, R. 1983. Symbols for rock-forming minerals. American Mineralogist: 68, 277–279.

Kohn, M. J., Spear, F. S. 1989. Empirical calibration of geobarometers for the assemblage: garnet + hornblende + plagioclase + quartz. American Mineralogist: 74, 77–84.

Krogh, J., Raheim A. 1978. Temperature and Pressure dependence of Fe-Mg partitioning between garnt and phengite with particular refrence to eclogite. Contributions to Mineralogy and Petrology: 66, 75–80.

Leake, B, E. 1997. Nomenclature of amphiboles. Report of the Sub- committee on Amphiboles of the International Mineralogical Association on New Minerals and Mineral Names. European Journal of Mineralogy: 9, 623–651.

Leake, B, E. 2003. Nomenclature of amphiboles: Additions and revisions to the international mineralogical association's 1997 recommendations. The Canadian Mineralogist: 41, 1355–1362.

Massone, H. J., Schryer, W. 1987. Phengitegeobarometry based on the limiting assemblage with k-feldspar, phlogopite and quartz. Contributions to Mineralogy and Petrology: 96, 212–224.

Mohajjel, M., Fergusson C. L. 2000. Dextral transpression in late Cretaceous continental collision, Sanandaj-Sirjan Zone, Western Iran. Journal of Structural Geology: 22, 1125–1139.

Mohajjel, M., Fergusson, C. L., Sahandi, M. R. 2003. Cretaceous-Tertiary convergence and continental collision, Sanandaj-Sirjan Zone, western Iran. Journal of Asian Earth Sciences: 21, 397–412.

Nelson, P., Jones, G. V., Snead, N. 2004. Geology and wine 8. Modelling viticultural landscapes: A GIS analysis. Geoscience Canada: 31, 167–178.

Perchuk, L. L., Podlesski, K. K., Aranovich , L. 1981. Calculation of thermodynamic properties of end member minerals from natural paragenesis in Newton. R. C., Navrotsky , A., and Wood. B. J., Thermoynamics of the mineral and melts : New York, Springer. P. 111–129.

Thompson, A. B. 1976, Mineral reactions in politic rocks. Calculation of some P-T-X (Fe-Mg) phase relations: American Journal of. Science: 276, 425–454.